Correlation energy functional from jellium surface analysis

Lucian A. Constantin,[1] Letizia Chiodo,[1] Eduardo Fabiano,[2] Igor Bodrenko,[2] and Fabio Della Sala[2,1]
[1]*Center for Biomolecular Nanotechnologies @UNILE, Istituto Italiano di Tecnologia, Via Barsanti, 73010 Arnesano (LE)*
[2]*National Nanotechnology Laboratory (NNL), Istituto Nanoscienze-CNR, Via per Arnesano 16, I-73100 Lecce, Italy*
(Received 12 April 2011; revised manuscript received 17 May 2011; published 18 July 2011)

Using the wave-vector analysis of the jellium exchange-correlation surface energy, we show that the PBEint generalized gradient approximation (GGA) of Fabiano *et al.* [Phys. Rev. B **82**, 113104 (2010)] is one of the most accurate density functionals for jellium surfaces, being able to describe both exchange and correlation parts of the surface energy, without error compensations. We show that the stabilized jellium model allows us to achieve a realistic description of the correlation surface energy of simple metals at any wave vector k. The PBEint correlation is then used to construct a meta-GGA correlation functional, modifying the one-electron self-correlation-free Tao-Perdew-Staroverov-Scuseria (TPSS) one. We find that this new functional (named JS) performs in agreement with fixed-node diffusion Monte Carlo estimates of the jellium surfaces, and is accurate for spherical atoms and ions of different spin-polarization and for Hooke's atom for any value of the spring constant.

DOI: 10.1103/PhysRevB.84.045126 PACS number(s): 71.10.Ca, 71.15.Mb, 71.45.Gm

I. INTRODUCTION

Kohn-Sham ground-state density-functional theory (DFT),[1,2] the most used method in first-principles electronic calculations of quantum chemistry and condensed-matter physics, is based on the approximations of the exchange-correlation (XC) energy (E_{xc}) and potential ($V_{xc,\sigma} = \delta E_{xc}/\delta n_\sigma$). Here n_σ is the spin density, $\sigma = \uparrow$ and $\downarrow$. In recent years, many XC functionals have been built, being classified on the so-called "Jacob's ladder."[3] The ground on which the ladder lies is the Hartree approximation (XC energy and potential are zero), and the first rung is the local spin-density approximation (LSDA) constructed entirely from the uniform electron-gas model:[1]

$$E_{xc}^{\mathrm{LSDA}} = \int d\mathbf{r}\; n\epsilon_{xc}^{\mathrm{unif}}(n_\uparrow, n_\downarrow), \tag{1}$$

where $\epsilon_{xc}^{\mathrm{unif}}(n_\uparrow, n_\downarrow)$ is the exchange-correlation energy per particle of an electron gas with uniform spin densities $n_\uparrow$ and $n_\downarrow$.[4,5]

The next rungs of the Jacob's ladder are the generalized gradient approximation (GGA) and the meta-GGA that use more ingredients in order to satisfy exact constraints of the XC energy:

$$E_{xc}^{\mathrm{GGA}} = \int d\mathbf{r}\; n\epsilon_{xc}^{\mathrm{GGA}}(n_\uparrow, n_\downarrow, \nabla n_\uparrow, \nabla n_\downarrow), \tag{2}$$

and

$$E_{xc}^{\mathrm{MGGA}} = \int d\mathbf{r}\; n\epsilon_{xc}^{\mathrm{MGGA}}(n_\uparrow, n_\downarrow, \nabla n_\uparrow, \nabla n_\downarrow, \tau_\uparrow, \tau_\downarrow), \tag{3}$$

where $\tau_\sigma(\mathbf{r})$ are the positive Kohn-Sham kinetic energy densities,

$$\tau_\sigma(\mathbf{r}) = \sum_i^{\mathrm{occ.}} \frac{1}{2} \mid \nabla\psi_{i\sigma}(\mathbf{r}) \mid^2, \tag{4}$$

and $\psi_{i\sigma}(\mathbf{r})$ are the occupied Kohn-Sham orbitals of spin σ. (Unless otherwise stated, atomic units are used throughout, i.e., $e^2 = \hbar = m_e = 1$.)

These approximations are nowadays the most used because of their computational efficiency and accuracy. Due to its simplicity, no GGA functional can be accurate for both atoms and solids.[6] In spite of this severe limitation, there are accurate GGAs for molecules (e.g., BLYP,[7] revPBE,[8] APBE,[9] PBE[10]), for solids (e.g., PBEsol,[11] AM05[12]), for surfaces (e.g., PBEsol, AM05, PBEint[13]), and for hybrid interfaces (e.g., PBEint). On the other hand, meta-GGA[14,15] can achieve good accuracy for solids, atoms, and molecules, and might overcome difficult problems in condensed-matter physics, as interaction of CO molecule with Pt surface.[16]

Higher rungs of the ladder, such as optimized effective potentials,[17–19] hyper-GGA, and random-phase approximation (RPA) methods have a nonlocal dependence of the Kohn-Sham orbitals, showing a prohibitively high computational cost. Moreover, the hyper-GGA, which is a fully nonlocal correlation functional compatible with exact exchange, has an important degree of empiricism, and even if it satisfies many exact constraints, it is not as accurate as it was expected.[20] The random-phase approximation (RPA) method is very expensive for a full self-consistent calculation, employing the occupied and unoccupied Kohn-Sham orbitals. Non-self-consistent RPA evaluations severely fail for Be_2 binding energy,[21] and unfortunately show an important dependence on the chosen orbitals[22] for molecules. This is not the case for bulk solids, for which RPA is remarkably accurate.[23] RPA-related methods, such as the inhomogeneous Singwi-Tosi-Land-Sjölander (ISTLS) approach,[24,25] or the ones derived from the linear response of time-dependent density-functional theory in the context of adiabatic-connection-fluctuation-dissipation theorem, have been barely applied to finite systems.

Jellium electron gas has become, along the years, a DFT paradigm used to construct and to test XC approximations, as well as to derive important exact properties of XC energy. Jellium is a simple model of a simple metal, in which the ion cores are replaced by a uniform positive background of density $\bar{n} = 3/4\pi r_s^3 = k_F^3/3\pi^2$, and the valence electrons in the spin-unpolarized bulk neutralize this background. Here r_s is the bulk density parameter ($r_s = 2.07$ for Al and 3.93 for Na), and k_F is the bulk Fermi wave vector. The jellium surface

energy (σ) is the energy cost per unit area to create a planar surface by cutting the bulk. Lang and Kohn[26] reported for the first time jellium surface LSDA self-consistent calculations that showed early evidence that density functionals may work for surface science. However, jellium XC surface energy (σ_{xc}) was a long-standing puzzle: density functionals, RPA, and time-dependent DFT methods[27] agree well with each other but disagree strongly with high-level correlated methods such as Fermi hypernetted chain (FHNC//0)[28] and old diffusion Monte Carlo (DMC)[29] calculations for jellium slabs. This puzzle was resolved by new DMC calculations,[30] by the inhomogeneous Singwi-Tosi-Land-Sjölander approach,[25] and by the jellium surface wave-vector analysis at the RPA level.[31] Indeed, all the semilocal rungs of the Jacob's ladder (LSDA, GGA, meta-GGA) are reliable for jellium surfaces.

The wave-vector analysis of jellium XC surface energy is an important tool for understanding how well an XC approximation works, because it separates the long-range and short-range XC effects. Langreth and Perdew[32] showed that the exact XC energy of any inhomogeneous system can be obtained from a three-dimensional (3D) Fourier transform (wave-vector analysis) of the spherical averaged XC hole density, that is, a function of a 3D wave vector **k**. For a jellium surface, exact constraints of this wave-vector-dependent XC hole are known: at long wavelengths ($k \to 0$) the surface plasmons dominate, whereas at short wavelengths ($k \to \infty$), LSDA becomes accurate.[32,33] These known limits have been used to carry out a wave-vector interpolation correction to LSDA,[32] PBE-GGA,[34] and TPSS-metaGGA.[35]

Moreover, recent 2D and 3D wave-vector analyses of the exact RPA,[31,36] ISTLS,[25] and time-dependent DFT (TDDFT)[27,37] calculations have been used to solve and understand the jellium surface problem, and as accurate benchmarks for density functionals.[13,31,37] Thus such calculations become a common test for density functionals, because they can reveal the accuracy of the approximation for the surface energy at any wave vector.

Recently, the PBEint GGA functional[13] for hybrid interfaces has been constructed, with the aim to preserve, as much as possible at the GGA level, the good properties of both PBE and PBEsol, i.e., a good description of molecular and solid-state properties, respectively. Its exchange enhancement factor is

$$F_x(s) = 1 + \kappa - \frac{\kappa}{1 + \mu(s)s^2/\kappa}, \tag{5}$$

where $s = |\nabla n|/[2(3\pi^2)^{1/3}n^{4/3}]$ is the reduced gradient, $\kappa = 0.804$ is fixed from the Lieb-Oxford bound,[10] and

$$\mu^{\mathrm{PBEint}}(s) = \mu^{\mathrm{GE}} + (\mu^{\mathrm{PBE}} - \mu^{\mathrm{GE}})\frac{\alpha s^2}{1 + \alpha s^2}, \tag{6}$$

with $\alpha = (\mu^{\mathrm{GE}})^2/[\kappa(\mu^{\mathrm{PBE}} - \mu^{\mathrm{GE}})] = 0.197$. Here $\mu^{\mathrm{GE}} = 10/81$ is the coefficient of the second-order gradient expansion (GE) of exchange energy, and $\mu^{\mathrm{PBE}} = 0.219\,51$ was derived from the linear response of bulk jellium, but is also reasonably accurate for heavy atoms.[6,9] The value of α was fixed from the constraint $d^2F_x^{\mathrm{PBEint}}(s)/d(s^2)^2|_{s=0} = 0$, which ensures a smooth functional derivative $\delta E_x^{\mathrm{PBEint}}/\delta n$. Equation (6) leads then to the recovery of the second-order gradient expansion of the exchange energy over a large range of the reduced gradient (for $s \lesssim 1$ PBEint exchange is close to PBEsol exchange).[13] In the rapidly varying density regime ($s \geqslant 2.5$), $\mu^{\mathrm{PBEint}} \to \mu^{\mathrm{PBE}}$, PBEint exchange behaves as PBE exchange. For the correlation functional, PBEint has a PBE-like expression with $\beta = 0.052$, fitted to jellium surfaces. A very similar value of β has been also found for the RGE2 functional,[38] which uses a different exchange functional. The PBEint is accurate for bulk solids and jellium surfaces because it recovers the second-order gradient expansion in the slowly varying limit, as well as for metal-molecule interfaces because it also recovers the PBE behavior at medium and large values of the reduced gradient s. Recently, good performance of the PBEint functional for the description of electronic and structural properties of gold nanostructures was also reported.[39]

PBEint GGA gives similar wave-vector analysis of the jellium XC surface energy as PBEsol.[13] However, in Sec. II, we show that, unlike PBEsol, PBEint does not rely on an error cancellation between the exchange and correlation parts of the jellium surface energy, being able to accurately account not only for σ_{xc} , but also for σ_x and σ_c separately, at every 3D wave vector k. By employing a reliable model for the simple metal surfaces (stabilized jellium model), we achieve a realistic picture of the correlation surface energy $\sigma_c(k)$ of Al (111), and we show significant differences from the jellium model. Our calculations give indication for the behavior of exact σ_{xc} and σ_c of real metal surfaces.

Because the PBEint correlation parameter $\beta = 0.052$ can capture the right physics of the exact correlation for jellium surfaces, and from this point of view is a nonempirical parameter, it can be used further in construction of more accurate approximations for the correlation hole and energy. Thus, in Sec. III, we modified the TPSS meta-GGA correlation functional,[14] which is self-correlation free for one-electron systems, to recover the PBEint correlation energy at slowly varying density regime, and at jellium surfaces. This new jellium-surface (JS) correlation functional is remarkably accurate for jellium surfaces, atoms, ions, and Hooke's atom. Finally in Sec. IV, we summarize our conclusions.

II. WAVE-VECTOR ANALYSIS OF JELLIUM AND STABILIZED JELLIUM XC SURFACE ENERGIES

In our calculations we use self-consistent LSDA orbitals and densities, as in Refs. 13, 31, 34, 35, and 37. It is fair and reasonable to compare the energies predicted by different functionals for the *same* density. Self-consistency effects on the density from corrections to LSDA are small for jellium, where the self-interaction errors are negligible, as shown in Figs. 1 and 2 of Ref. 40 and Fig. 1 of Ref. 41. Moreover, because LSDA orbitals give very good results in describing jellium surfaces,[37] we also use them for the stabilized jellium calculations (see Sec. II B below), similar to Ref. 42.

A. Jellium

Let us consider a jellium surface at $z = 0$. This system is translationally invariant in the plane perpendicular to the z axis.

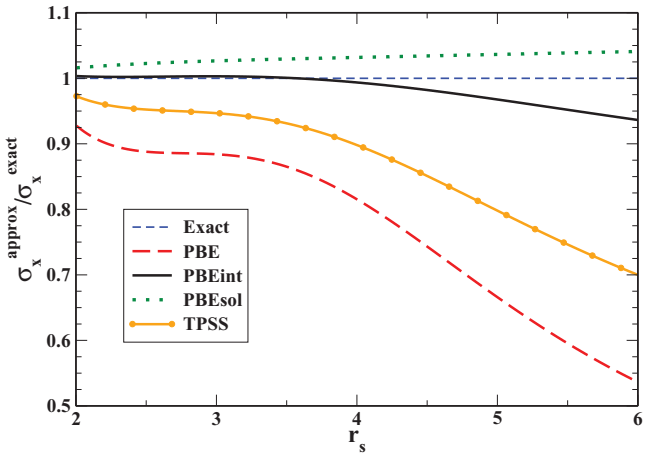

FIG. 1. (Color online) Comparison of the PBE, TPSS, PBEsol, and PBEint exchange-only jellium surface energies with the exact results. σ_x^{exact} were calculated in Ref. 36, using the adiabatic-connection-fluctuation-dissipation theorem.

This symmetry greatly simplifies the Kohn-Sham equations because $v_{\rm eff}(\mathbf{r}) = v_{\rm eff}(z)$, and the normalized orbitals become

$$\Phi_{\mathbf{k}_{||},l}(\mathbf{r}) = \frac{1}{A^{1/2}} e^{i\mathbf{k}_{||}\mathbf{r}_{||}} \phi_l(z), \tag{7}$$

where A is the cross-sectional area, $\mathbf{k}_{||}$ and $\mathbf{r}_{||}$ are the wave vector and the position in the plane perpendicular to the z axis, and $\phi_l(z)$ are solutions of the one-dimensional Kohn-Sham equations,

$$\left[-\frac{1}{2}\frac{d^2}{dz^2} + v_{\rm eff}(z)\right]\phi_l(z) = \epsilon_l \phi_l(z), \tag{8}$$

with $l = 1,2,\ldots,l_M$ is the subband quantum number (l_M is the highest occupied level) for a jellium slab, and l is a continuous quantum index in the case of an infinite jellium surface.[26]

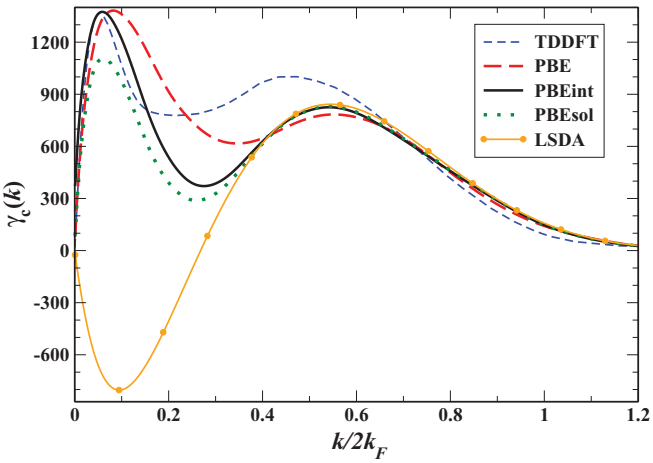

FIG. 2. (Color online) LSDA, PBE, PBEsol, PBEint, and TDDFT wave-vector-resolved correlation surface energies $\gamma_c(k)$, versus $k/2k_F$, for a jellium slab of thickness $a = 2.23\lambda_F$ and $r_s = 2.07$. The area under each curve represents the corresponding correlation surface energy; see Table I.

TABLE I. PBE, PBEint, PBEsol, TDDFT, and DMC jellium surface correlation energies (erg/cm^2) of the slabs shown in Figs. 2 and 3. The DMC values are extrapolated for every slab, taking into account the quantum size effects of the slabs. The values which best agree with DMC ones are indicated with bold font. (1 hartree/bohr^2 = 1.557 × 10^6 erg/cm^2.)

	PBE	PBEint	PBEsol	TDDFT	DMC
$r_s = 2.07$	720	**661**	604	742	674 ± 45
$r_s = 3$	262	**233**	220	275	230 ± 10

Because the sums over $\mathbf{k}_{||}$ can be done analytically in many calculations[36] due to

$$\frac{1}{A}\sum_{\mathbf{k}_{||}} \longrightarrow \int \frac{d^2\mathbf{k}_{||}}{(2\pi)^2}, \tag{9}$$

the jellium surface becomes in principle a one-dimensional problem.

The surface exchange-correlation energy is[26,34]

$$\begin{aligned}\sigma_{xc} &= \int_{-\infty}^{\infty} dz\, n(z)\{\epsilon_{xc}([n];z) - \epsilon_{xc}^{\rm unif}(\bar{n})\} \\ &= \int_0^{\infty} d\left(\frac{k}{2k_F}\right)\gamma_{xc}(k),\end{aligned} \tag{10}$$

where $\gamma_{xc}(k)$ is the 3D wave-vector analysis, that is,

$$\gamma_{xc}(k) = \int_0^{\infty} du\; 8k_F u^2 b_{xc}(u)\sin(ku)/(ku), \tag{11}$$

where

$$b_{xc}(u) = \int_{-\infty}^{\infty} dz\, n(z)\{n_{xc}([n];z,u) - n_{xc}^{\rm unif}(\bar{n};u)\}, \tag{12}$$

where $n_{xc}([n];z,u)$ is the spherical average of the coupling-constant averaged XC hole density.[31,37] Here the 3D wave vector k is defined as $k = \sqrt{\mathbf{k}_{||}^2 + k_z^2}$.

The exact low-wave-vector limit of γ_{xc} is[32]

$$\gamma_{xc}(k \to 0) = \frac{k_F}{4\pi}\left(\omega_s - \frac{1}{2}\omega_p\right)k, \tag{13}$$

where $\omega_p = (4\pi\bar{n})^{1/2}$ and $\omega_s = \omega_p/\sqrt{2}$ are the bulk- and surface-plasmon energies, and $\bar{n}$ is the bulk density. The exact high-wave-vector limit of γ_{xc} is not known, but LSDA is very accurate in this limit[32,33] of short-wavelength oscillations.

In Fig. 1 we show a comparison of σ_x at semi-infinite jellium surfaces, for various density functionals, in the range $2 \leqslant r_s \leqslant 6$ where most of the metals lie. In these calculations, we use the physically motivated Eq. (15) of Ref. 41 to interpolate or extrapolate to any r_s (solving four linear equations fitted at $r_s = 2, 3, 4$, and 6). The exact values $\sigma_x^{\rm exact}$ for $r_s = 2, 3, 4$, and 6 are taken from Table II of Ref. 36. Similar calculations were already reported (see Ref. 35 and Fig. S3 of the supplementary material of Ref. 11).

Both PBEsol and PBEint are very accurate for any r_s, but PBEint is almost exact in the range $2 \leqslant r_s \leqslant 4$, outperforming all other functionals. We recall that $\sigma_{xc}^{\rm PBEint} \approx \sigma_{xc}^{\rm PBEsol} \approx \sigma_{xc}^{\rm TPSS} \approx \sigma_{xc}^{\rm DMC}$, where $\sigma_{xc}^{\rm DMC}$ are the fixed-node diffusion Monte Carlo (DMC) calculations of Ref. 30. (See also Table II of Ref. 25.) Thus while TPSS meta-GGA and PBEsol GGA

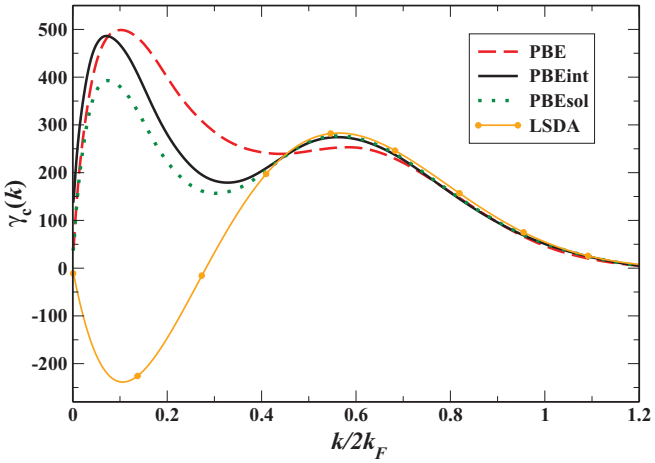

FIG. 3. (Color online) Same as Fig. 2, but for a jellium slab of thickness $a = 2.23\lambda_F$ and $r_s = 3$. The area under each curve represents the corresponding correlation surface energy; see Table I.

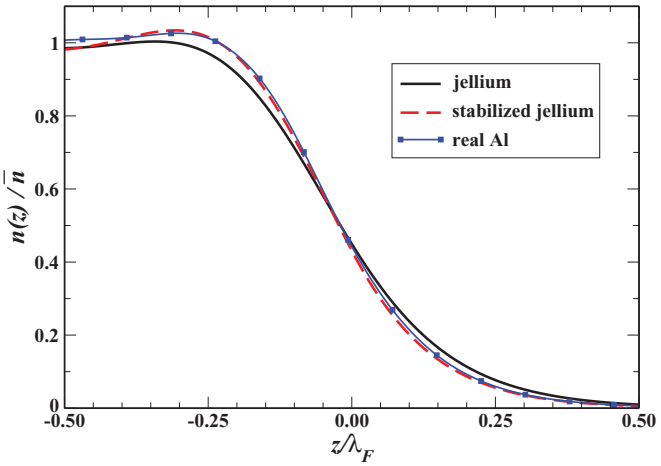

FIG. 4. (Color online) Normalized valence electrons densities of the jellium and stabilized jellium models, at a semi-infinite surface of $r_s = 2.07$ versus z/λ_F. Also shown is the density of a thick (11-layer) real Al slab. The surface plane is at $z = 0$, the bulk is at $z \leqslant 0$, and the vacuum is at $z \geqslant 0$.

rely on an error compensation between σ_x and σ_c, PBEint gives very accurate results for both σ_x and σ_c.

In order to understand better the PBEint behavior at jellium surfaces, we perform the wave-vector analysis of Eq. (11). The LSDA, PBE, PBEsol, and PBEint exchange-correlation hole functions are accurately known. See Refs. 4, 43, and 44 for the LSDA exchange-correlation hole, Ref. 43 for the smoothed PBE exchange hole model and Ref. 45 for the PBE correlation hole, Ref. 37 for PBEsol XC hole density, and Ref. 13 for PBEint XC hole density.

In Ref. 13, it was shown that $\gamma_{xc}^{\mathrm{PBEint}}(k)$ agrees very well with $\gamma_{xc}^{\mathrm{PBEsol}}(k)$, being between the most accurate GGAs for surface energies. A detailed comparison of PBE, PBEsol, and exact jellium exchange surface energies was reported in Fig. 6 of Ref. 37. However, the nonoscillatory model of the GGA exchange hole is inaccurate near $k = 2k_F$. Thus we focus only on the correlation part. We choose two jellium slabs of the same thicknesses $a = 2.23\lambda_F$ and $r_s = 2.07$ (which corresponds to Al) and $r_s = 3$, respectively. These slabs have been used also in Refs. 31 and 37.

In Fig. 2, we show a comparison of $\gamma_c(k)$ for several density functionals and for a sophisticated TDDFT calculation[37] that uses the adiabatic-connection-fluctuation-dissipation theorem. The TDDFT curve is exact at low wave vectors and high wave vectors, but gives surface correlation energies similar with the RPA ones,[27] e.g., considerably higher than the DMC benchmarks results (see Table I). Thus we use TDDFT calculation for comparison only in the low- and high-wave-vector regimes.

$\gamma_c(k)^{\mathrm{PBEint}}$ is remarkably close to $\gamma_c(k)^{\mathrm{TDDFT}}$ in both low- and high-wave-vector regions, and its integrated surface correlation energy agrees best with the DMC data (Table I). These facts indicate that $\gamma_c(k)^{\mathrm{PBEint}}$ is the most accurate curve of Fig. 2, showing that the parameter $\beta = 0.052$ used in the construction of PBEint correlation captures the behavior of the *exact* correlation energy for simple metals. The same PBEint good behavior is shown in Fig. 3, for the jellium slab with $r_s = 3$.

Note that even if the PBEint correlation parameter ($\beta = 0.052$) is between the PBE ($\beta = 0.0667$) and PBEsol ($\beta = 0.046$) values, inspection of Figs. 2 and 3 shows that PBEint has the steepest curve in the plasmonic region ($k/2k_F \to 0$). Moreover, $\gamma_c^{\mathrm{PBEint}}(k)$ correctly recovers the right $\gamma_c^{\mathrm{TDDFT}}(k)$ at small k, $\gamma_c^{\mathrm{LSDA}}(k)$ at large k, and $\int_0^\infty dk\gamma_c^{\mathrm{PBEint}}(k)$ is the most accurate. Thus $\beta = 0.052$ can be considered an (almost) exact correlation hole constraint for jellium surfaces.

B. Stabilized jellium

In the last subsection we have found that PBEint is very accurate for the ideal, jellium surfaces. However, the jellium model has serious deficiencies in describing simple metals: for $r_s \approx 2$ the jellium total surface energy σ is negative, and for $r_s \approx 6$, the jellium bulk modulus is negative. These limitations were solved in the stabilized jellium model,[46] by taking into account the interaction between the ions and electrons through a simple empty-core pseudopotential as

$$w(r) = \begin{cases} -z/r, & r \geqslant r_c \\ 0, & r < r_c, \end{cases} \tag{14}$$

and by eliminating the spurious self-repulsion energy of the positive background in each cell.[46] Here z is the ion charge, and r_c is the core radius, which is defined by Eq. (26) of Ref. 46. (The corresponding parameters for the simple metal Al are $r_s = 2.07$, $r_c = 1.11$, and $z = 3$.) In the practical implementation of the model, to avoid the need to exactly define the bulk structure, the stabilized jellium model is turned into a simple structureless pseudopotential model. This is achieved by taking the difference between the pseudopotential and the electrostatic potential of the jellium positive background to be constant in the bulk (averaging over a Wigner-Seitz cell) and zero outside (see Sec. II of Ref. 46). The stabilized jellium model gives accurate surface energies of simple metals (see Fig. 2 of Ref. 46) and, moreover, the remaining small discrepancy with real surfaces can be corrected by including geometric effects using a "corrugation factor."[46,47]

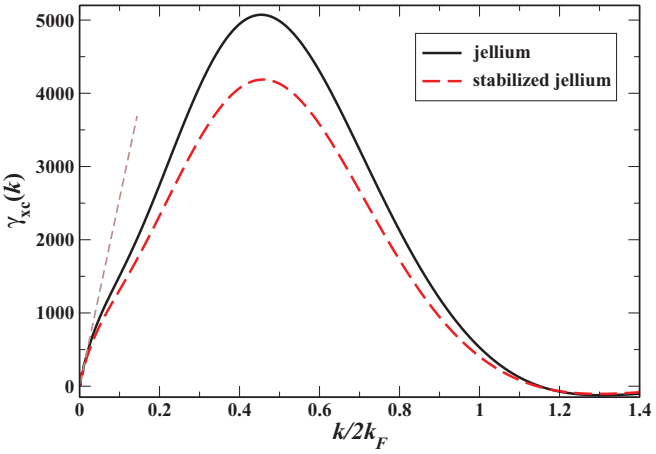

FIG. 5. (Color online) PBEint wave-vector-resolved XC surface energies $\gamma_{xc}(k)$ versus $k/2k_F$, for semi-infinite jellium and stabilized jellium surfaces. The bulk parameter is $r_s = 2.07$. The exact slope is given by Eq. (13). The area under each curve represents the corresponding XC surface energy; see Table II.

In Fig. 4 we show the normalized densities $n(z)/\bar{n}$ at the semi-infinite jellium, semi-infinite stabilized jellium, and 11-layer-slab real Al surfaces. The calculation for real Al was done at the PBEint self-consistent level (LSDA gives a similar density), and computational details are given in the next subsection. Figure 4 confirms that the stabilized jellium density is steeper[46] and agrees in detail with the valence density of real metal, showing that the electrons near the surface are more tightly bounded than in the jellium model case. For a slab, the same behavior can be seen in Fig. 1 of Ref. 42.

Because the stabilized-jellium model is an appropriate model for real surfaces, it is thus important to understand how the wave-vector analysis is modified in this more realistic case. We thus report a comparison of the $\gamma_{xc}(k)$ and $\gamma_c(k)$ for jellium and stabilized jellium of semi-infinite surfaces of $r_s = 2.07$, at the PBEint level. Stabilized jellium model calculations use the regular bulk density $\bar{n}$.

In Fig. 5 we show that $\gamma_{xc}(k)$ of the stabilized jellium is always smaller than the jellium one. Moreover, both curves recover the exact behavior at $k \to 0$ [see Eq. (13)], and the accurate LSDA at $k \to \infty$. Thus a steeper density decreases considerably σ_x, whereas σ_c remains almost constant, as shown in Table II.

Finally, we show in Fig. 6 the surface correlation behavior. Even if the integrated σ_c agree well for both jellium and stabilized jellium (see Table II), their wave-vector analyses show qualitative differences: (i) the plasmonic region (small values of k) is more important for the stabilized jellium (and consequently in real simple metals); (ii) the short-wavelength ($k \to \infty$) region is less important for real surfaces, and (iii) at intermediate wave vectors, the variation of σ_c decreases in the stabilized jellium model.

TABLE II. PBEint semi-infinite jellium and stabilized jellium correlation and XC surface energies (erg/cm^2), for bulk parameter $r_s = 2.07$.

	Jellium	Stabilized jellium
σ_c	678	667
σ_{xc}	2984	2481

C. Simple metal: Aluminium

In this last subsection we present results for the real Al(111) surface, studied in the full self-consistent Kohn-Sham scheme, with PBE, PBEsol, and PBEint functionals. The calculations are performed within DFT, in a plane-wave pseudopotential approach.[48] Symmetric slabs of 11 layers thickness have been used, allowing all layers to relax in the direction perpendicular to the surface. Ultrasoft pseudopotentials with a cutoff of 35 Ry, a $10 \times 10 \times 1$ k-point grid, and a vacuum region of 14 Å thick have been employed. Surface energies were computed following Ref. 49.

In Table III we show the equilibrium lattice constant, bulk modulus, and surface energy of Al(111). The experimental values of the bulk modulus and lattice constants have been corrected for finite temperature and phonon zero-point effects, according to the careful analysis of Refs. 50 and 51. Note that these corrections are more than 7% for bulk moduli.

For the equilibrium lattice constant PBE is in very good agreement with experiments. This fact shows that in the Al bulk, there are important regions with relatively high values of the reduced gradient s. We also recall that the maximum value of s in Al (111) bulk is $s^{\max} = 1.4$, considerably higher than in other bulk solids. (See Table III of Ref. 52). For bulk modulus, both PBEint and PBEsol are accurate, being very close to the corrected experimental value.

For the real surface, PBEint and PBEsol give similar results, much better than the PBE one. This trend is in accord with our jellium surface calculations. We recall that for Al(111), the jellium surface is completely wrong ($\sigma = -642$ erg/cm^2), the stabilized jellium gives $\sigma = 801$ erg/cm^2, and the stabilized jellium together with a corrugation factor [see Eq. (56) of Ref. 46] gives $\sigma = 921$ erg/cm^2,[46] very close to our full DFT calculations and to the experimental value.

Clearly the good performance of the PBEint functional is not only related to the β coefficient, as the results in Table III take also into account exchange and self-consistent effects. Nevertheless, these results show that the PBEint functional yields a very accurate description of simple metals, being more accurate than PBEsol for lattice constant and more accurate than PBE for surface energies and bulk modulus.

TABLE III. Equilibrium lattice constant, bulk modulus, and surface energy of Al(111) from PBE, PBEint, and PBEsol self-consistent calculations. The experimental data were corrected for thermal and zero-point effects (see Table I of Ref. 51). The uncorrected experimental data are presented in brackets. The best results for each row are in bold font.

	PBE	PBEint	PBEsol	Expt.	
a_0 (Å)	**4.025**	4.009	3.998	4.022	(4.05)
B (GPa)	77.26	**81.78**	81.90	81.3	(76)
σ(erg/cm^2)	888	1027	**1035**	1140	

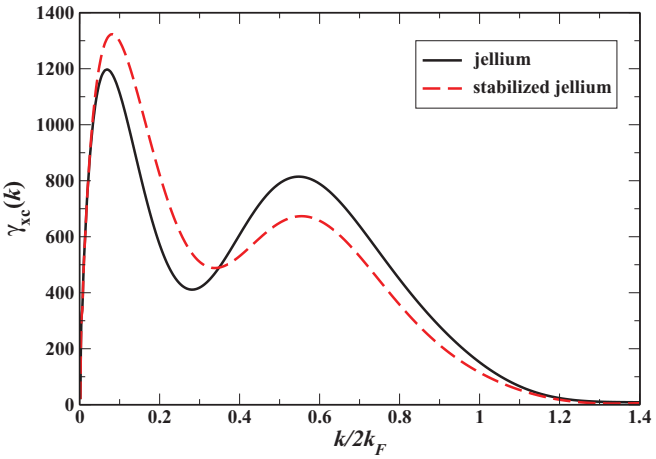

FIG. 6. (Color online) PBEint wave-vector-resolved correlation surface energies $\gamma_c(k)$ versus $k/2k_F$, for semi-infinite jellium and stabilized jellium surfaces. The bulk parameter is $r_s = 2.07$. The area under each curve represents the corresponding correlation surface energy; see Table II.

III. META-GGA CORRELATION FUNCTIONAL

In the previous section we showed that the PBEint parameter $\beta = 0.052$ correctly describes the correlation in simple metals. In this sense, $\beta = 0.052$ is a nonempirical parameter that can be used further in developing approximations on the higher rungs of the Jacob's ladder for both XC energy and hole.

In this section we propose the jellium surface (JS) meta-GGA correlation functional that is in fact a self-correlation correction to the PBEint GGA correlation, and is constructed in a similar way as TPSS and revTPSS meta-GGA correlation functionals.[14,15,53]

A. Construction of JS correlation functional

The meta-GGA correlation energy is[14,53]

$$E_c^{\mathrm{MGGA}} = \int d\mathbf{r}\, n\epsilon_c^{\mathrm{rev}}\left[1 + d\epsilon_c^{\mathrm{rev}} z^q\right], \tag{15}$$

where

$$z = \frac{\tau^W}{\tau}, \tag{16}$$

with $\tau^W = |\nabla n|^2/(8n)$ being the von Weizsäcker kinetic-energy density[2] and τ is the total Kohn-Sham positive kinetic-energy density [see Eq. (4)]. $\epsilon_c^{\mathrm{rev}}$ is a revision of PKZB meta-GGA correlation functional,[54] and has the general form

$$\epsilon_c^{\mathrm{rev}} = \epsilon_c^{\mathrm{GGA}}[1 + C(\zeta,\xi)z^m] - [1 + C(\zeta,\xi)]z^m \sum \frac{n_\sigma}{n}\tilde{\epsilon}_c^\sigma, \tag{17}$$

with

$$\tilde{\epsilon}_c^\sigma = \max\left[\epsilon_c^{\mathrm{GGA}}(n_\sigma,0,\nabla n_\sigma,0), \epsilon_c^{\mathrm{GGA}}(n_\uparrow,n_\downarrow,\nabla n_\uparrow,\nabla n_\downarrow\right]. \tag{18}$$

Here

$$\zeta = \frac{n_\uparrow - n_\downarrow}{n}, \quad \xi = \frac{|\nabla\zeta|}{2(3\pi^2 n)^{1/3}} \tag{19}$$

are the relative spin polarization and its reduced gradient.

For any $C(\zeta,\xi)$, d, and positive integers q and m, $E_c^{\mathrm{MGGA}} = 0$ for *any fully spin-polarized one-electron density* (defined by $\zeta = 1$ and $z = 1$). In the TPSS case, GGA = PBE, $q = 3$, and $m = 2$ (which represent minimum values for these parameters in order to satisfy exact constraints, such as recovery of gradient expansion). revTPSS also uses $q = 3$ and $m = 2$, but has a GGA expression similar to PBE but β is r_s dependent [see Eq. (3) of Ref. 15] with, e.g., $\beta(r_s = 2) = 0.059$, $\beta(r_s = 4) = 0.0546$, and $\beta(r_s = 6) = 0.0517$. The revTPSS parametrization of β is a fit to the exact $\beta(r_s)$ parameter of the second-order gradient expansion of the correlation energy, derived by Hu and Langreth.[55]

For JS we chose GGA = PBEint, and $q = m = 4$, such that in the slowly varying density regions, JS recovers faster the PBEint behavior. This choice was motivated by our observation that for jellium surfaces the PBEint correlation is a remarkably good choice.

For the uniform density scaling

$$n_\gamma(\mathbf{r}) = \gamma^3 n(\gamma\mathbf{r}), \quad \gamma > 0, \tag{20}$$

in the low-density limit ($\gamma \to 0$), the JS meta-GGA scales correctly as $E_c^{\mathrm{JS}} = \gamma W^{\mathrm{PBEint}}$, where W^{PBEint} is a negative constant given by using the value $\beta = 0.052$ in Eq. (39) of Ref. 53. In the high-density limit ($\gamma \to \infty$), E_c^{JS} correctly scales to a negative, n-dependent constant. In the large gradient limit ($s \to \infty$), JS correctly vanishes. In the slowly varying limit (small s), JS recovers PBEint correlation.

We find $C(\zeta,\xi)$ and d similar as in TPSS construction:[53] $C(0,0)$ and d are fixed by the requirement that for jellium surfaces, where the self-interaction error is negligible and PBEint works very well, JS recovers PBEint for any r_s. The spin-dependent behavior of $C(\zeta,\xi)$ is instead fixed by requiring that for a Wigner crystal jellium the correlation is independent of ζ for $0 < \zeta < 0.7$. This is obtained in practice by considering one-electron Gaussian densities of different spin polarization $0 < \zeta < 1$. Thus we propose the following:

$$d = 3.7, \tag{21}$$

and

$$C(\zeta,\xi) = \frac{0.353 + 0.87\zeta^2 + 0.5\zeta^4 + 2.26\zeta^6}{\left\{1 + \frac{1}{2}\sqrt{\xi}[(1+\zeta)^{-4/3} + (1-\zeta)^{-4/3}]\right\}^4}. \tag{22}$$

The denominator of Eq. (22) is a dumping factor dependent on $\sqrt{\xi}$. In the case of an electron gas with slowly varying spin densities, the gradient expansion of the correlation energy is known to contain terms depending on $|\nabla\zeta|^2$ and $\nabla n \cdot \nabla\zeta$ (which, however, negligibly contribute to the correlation energy[56]), but not on $\sqrt{\xi}$. Nevertheless, we can state that our construction is correct, because $\epsilon_c^{\mathrm{JS}} \to \epsilon_c^{\mathrm{PBEint}}$ in the slowly varying limit due to the choice $q = m = 4$. The denominator of Eq. (22) is thus only required to account for self-correlation in atoms.

In Fig. 7, we show the correlation energy per particle ϵ_c of TPSS, JS, and PBEint for the Li atom and the Ar^{15+} ion, versus the radial distance from the nucleus. For both atoms, $\epsilon_c^{\mathrm{TPSS}}$ and ϵ_c^{JS} are correctly zero in the monovalent region, where the self-correlation correction removes the PBEint bad behavior.

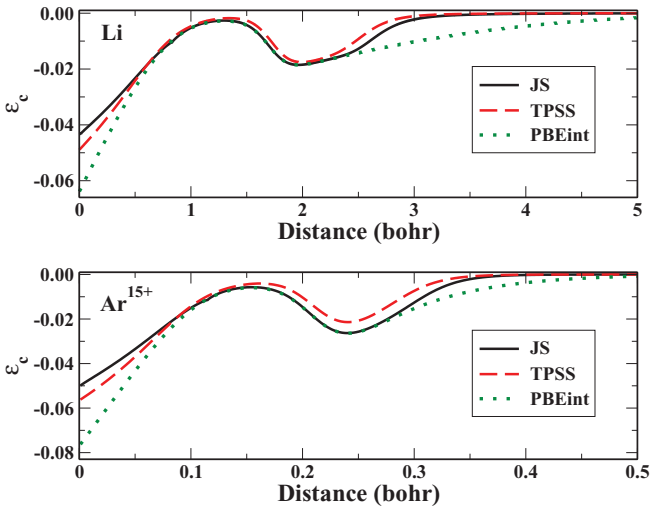

FIG. 7. (Color online) Correlation energy per electron (hartree) versus the radial distance r (bohr) from the nucleus, for Li atom (upper panel), and for Ar^{15+} (lower panel).

In Table IV, we report correlation energies of the one-electron Gaussian densities with different spin polarization ζ. All meta-GGAs are correct for $\zeta = 1$, and all of them give correlation energies practically independent on ζ in the range $0 \leqslant \zeta \leqslant 0.7$. These results reveal that JS can accurately describe correlation energies of low-density Wigner crystals, where the electrons are localized near the lattice sites.

B. Results

1. Jellium surfaces

In Table V we show that JS is very accurate for jellium surfaces, all the correlation values being in the range of DMC estimations. Moreover, JS and PBEint have similar performance, showing that our self-interaction correction correctly does not have any effect for jellium surfaces, where the electrons are delocalized. TPSS and PBE overestimate the jellium surface correlation energies, and PBEsol underestimates them for $2 \leqslant r_s \leqslant 3$. Thus the most accurate values in Table V, all in the range of DMC calculations, are given by revTPSS, JS, and PBEint.

TABLE IV. Correlation energies (hartree) of the one-electron Gaussian densities with relative spin-polarization ζ.

ζ	TPSS	revTPSS	JS
0.0	−0.021	−0.022	−0.019
0.1	−0.021	−0.022	−0.019
0.2	−0.020	−0.022	−0.019
0.3	−0.020	−0.022	−0.019
0.4	−0.020	−0.021	−0.019
0.5	−0.020	−0.021	−0.019
0.6	−0.019	−0.021	−0.019
0.7	−0.018	−0.020	−0.018
0.8	−0.017	−0.018	−0.017
0.9	−0.012	−0.013	−0.013
1.0	0.000	0.000	0.000

TABLE V. Semi-infinite jellium surface correlation energies (erg/cm^2) for PBE, PBEint, and PBEsol GGA functionals and TPSS, revTPSS, and JS meta-GGA functionals. Results within the DMC error bar are denoted with boldface.

r_s	PBE	PBEint	PBEsol	TPSS	revTPSS	JS	DMC
2	829	**745**	708	827	**771**	**749**	768 ± 50
3	276	**246**	**234**	274	**251**	**248**	242 ± 10
4	124	**111**	**105**	125	**111**	**112**	104 ± 8
6	40.2	35.4	33.3	39.6	34.8	35.9	31 ±...

2. Hooke's atom

To further assess the JS meta-GGA correlation functional we consider in this subsection Hooke's atom. This model system represents two interacting electrons in an isotropic harmonic potential of frequency ω. The XC wave-vector analysis of the Hooke's atom is different from the jellium surfaces, because in the large k limit ($k \to \infty$), the LSDA is not accurate.[33] Thus this system is a challenging test for the JS meta-GGA. Moreover, at small values of ω, the electrons are strongly correlated, and at large values of ω, they are tightly bound, two important cases in many condensed-matter applications.

The exact ground-state solutions of the Hooke's atom correlated wave function are known:[57] Introducing the center of mass $\mathbf{R} = (\mathbf{r}_1 + \mathbf{r}_2)/2$, and the relative coordinate $\mathbf{r} = \mathbf{r}_1 - \mathbf{r}_2$, the two-particle Hamiltonian is separable, and the Schrödinger equation decouples in two separate equations depending only on $\mathbf{R}$ and $\mathbf{r}$, respectively [see Eqs. (6) and (7) of Ref. 57].

The center of mass behaves as a 3D harmonic oscillator of frequency $\omega_{\mathbf{R}} = 2\omega$,[57] whose solution is well known. The eigenvalue problem for the relative motion is[57]

$$\left[-\frac{1}{2}\nabla_{\mathbf{r}}^2 + \frac{1}{2}\omega_r^2 r^2 + \frac{1}{2r}\right]\phi(\mathbf{r}) = \epsilon\phi(\mathbf{r}), \tag{23}$$

with $\omega_r = \omega/2$. Exact analytical ground-state solutions of Eq. (23) are known for *special* values of ω.[57] They have the form

$$\phi(\mathbf{r}) = \phi(r) \sim \frac{u(r)}{r}, \tag{24}$$

where

$$u(r) = e^{-\rho^2/2}\rho\sum_{v=0}^{p-1} a_v \rho^v, \tag{25}$$

with $\rho = \sqrt{\omega_r} r$, and p an integer ($p \geqslant 2$). For any $p \geqslant 2$, Eqs. (24) and (25) provide an exact ground-state solution, whose corresponding ω is obtained from a nonlinear equation [see Eq. (25) of Ref. 57]. Thus there is a one-to-one correspondence between the special values of ω for which analytical ground state [Eqs. (24) and (25)] exists, and the power of the polynomial p that defines this ground state.

Let us consider the classical electron distance[57]

$$r_0 = \left(2\omega_r^2\right)^{-1/3}, \tag{26}$$

which plays a similar role as λ_F in the case of jellium surfaces. In Fig. 8 we show the normalized exact ground-state densities $n(r)r_0^3$ for different frequencies. The solutions with

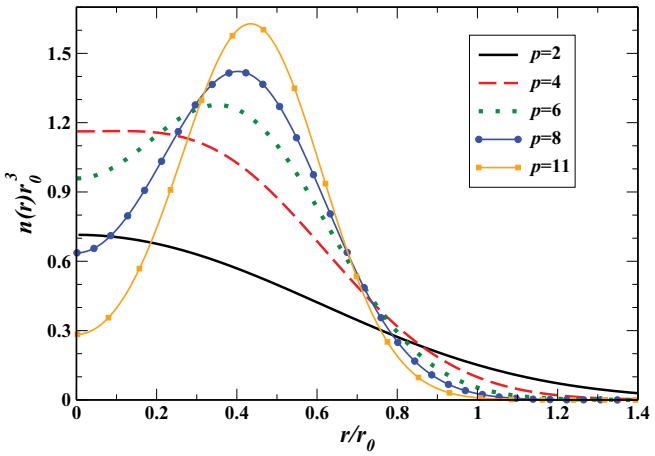

FIG. 8. (Color online) Exact normalized ground-state electron densities $n(r)r_0^3$ of the Hooke's atom with different frequencies, versus the radial distance r/r_0. Here r_0 is the classical electron distance defined in Eq. (26). p represents the order of the polynomial of Eq. (25). For $p = 2$, $r_0 = 2$; for $p = 4$, $r_0 = 11.4425$; for $p = 6$, $r_0 = 27.9349$; for $p = 8$, $r_0 = 51.5285$; and for $p = 11$, $r_0 = 100.2476$. In all cases, $\int_0^\infty dr 4\pi r^2 n(r) = 2$.

$2 \leqslant p \leqslant 4$ [see Eq. (25)] represent the low-correlation regimes (or tightly bounded regimes), and the solutions with $p \geqslant 8$ are the strongly correlated regimes. In the strong-correlated case, the region near the "nucleus" of the Hooke's atom has a deep "hole" due to the strongly correlated electrons, and, moreover, the density becomes more localized over a r_0 length. As $p \to \infty$, the electrons are perfectly localized around r_0 (note that in this case $r_0 \to \infty$).

We calculate the exact correlation energies for the first ten ground-state exact solutions of the Hooke's atom ($2 \leqslant p \leqslant 11$), using the same procedure described in Ref. 58. Our exact correlation results are reported in the lower panel of Fig. 9.

In the upper panel of Fig. 9, we show the accuracy of several correlation functionals. We use the exact densities and orbitals. As we mentioned at the beginning of Sec. II, it is a common, fair practice to test different functionals for the *same* density.

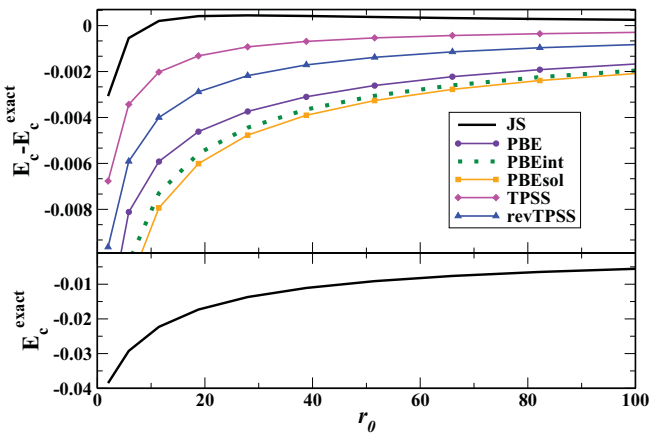

FIG. 9. (Color online) Upper panel: Errors of several correlation functionals $E_c^{\text{approx}} - E_c^{\text{exact}}$ (hartree) versus the classical electron distance r_0. Lower panel: Exact correlation energy E_c^{exact} (hartree) versus the classical electron distance r_0 (bohr).

For these unpolarized systems, $\tau = \tau^W$ so $z = 1$, and $\zeta = 0$, and thus the construction of $C(0,0)$ and d becomes essential for describing this two-electron system. The JS meta-GGA is very accurate over the whole frequency regimes, including tightly bounded and strongly correlated ones,[58,59] outperforming all the other approximations.

These results, which are not related to jellium surfaces, show that JS meta-GGA may be one of the most accurate correlation functionals for many-electron systems.

3. *Atoms and ions*

Finally, we consider briefly an application to real systems, employing the JS correlation functional to compute the correlation energy of several atoms. A more comprehensive study of real systems (e.g., molecules) is beyond the scope of this work and will be the subject of a future investigation.

In Table VI we report the correlation energy per electron E_c/N of 15 spin-unpolarized spherical atoms and ions (Ar^{6+}, Ar, Kr, Xe, Zn, two-electron systems: He, Li^+, Be^{2+}; four-electron systems: Be, B^+, C^{2+}, N^{3+}, O^{4+}; and ten-electron systems: Ne, Ar^{8+}), and 11 spin-polarized spherical atoms and ions (H, N, O^+, and three-electron systems: Be^+, Li, Ar^{15+}, C^{3+}, N^{4+}, B^{2+}, O^{5+}, Ne^{7+}). We use analytic Hartree-Fock densities and orbitals.[60]

For spin-unpolarized systems, all functionals give rather similar results with differences of few mHa per electron. None of the investigated functionals shows a clearly superior performance, nevertheless, the JS and PBEint functionals give overall the best mean absolute error (MAE) and mean absolute relative error (MARE). This shows that PBEint and JS better describe the correlation.

For spin-polarized systems, on the other hand, the JS functional clearly outperforms the other functionals yielding always the best agreement with the reference values, except for the O^+ atom, and the best overall performance with a MAE of 1.1 mHa per electron. This result provides an indication for the accuracy of Eq. (22).

IV. CONCLUSIONS AND FUTURE PERSPECTIVES

In this paper we have shown that the PBEint correlation functional accurately describes jellium surfaces at any wave vector k, giving a very accurate surface wave-vector analysis not only for total XC energy, but also for exchange and correlation parts. Thus at the simple but accurate PBEint GGA level, we have performed a wave-vector analysis of stabilized jellium, which is a realistic model of simple metals, and we have obtained a good description of surface energies of simple metals at any wave vectors. We have found qualitative differences between jellium and stabilized jellium correlation surface energies, which are reported in Figs. 5 and 6. These findings should be a starting point for the investigation of other differences between jellium and real metals, e.g., the asymptotic behaviors of XC energy per particle, and XC potential far outside the surface.[63,64]

We have shown that the PBEint correlation parameter $\beta = 0.052$ captures the exact physics of jellium surfaces, and is thus an exact hole constraint. Further, we have performed a self-interaction correction to the PBEint correlation, by

TABLE VI. Correlation energies per electron (E_c/N, mHa) of spherical atoms and ions with Hartree-Fock analytic orbitals and densities (Ref. 60). Best results are indicated in boldface.

Atom	PBE	PBEint	PBEsol	TPSS	revTPSS	JS	Ref.
			Spin-unpolarized atoms and ions				
He	**−21.0**	−24.5	−26.3	−21.5	−23.1	−21.1	−21.0[a]
Li^{+}	**−22.4**	−26.4	−28.3	−22.8	−24.3	−22.5	−21.7[a]
Be^{2+}	**−23.1**	−27.2	−29.3	−23.5	−24.7	−23.2	−22.2[a]
Be	−21.4	−24.6	−26.1	−21.7	**−23.1**	−21.7	−23.6[a]
B^{+}	−23.0	−26.5	**−28.2**	−23.4	−24.7	−23.6	−27.8[a]
Ne	−35.1	**−39.2**	−41.2	−35.4	−36.5	−38.0	−39.1[a]
Ar	−39.3	−43.5	−45.5	−39.5	**−40.5**	−42.6	−40.1[a]
Kr	−49.1	−53.8	**−56.0**	−49.2	−49.9	−53.3	−57.4[b]
Xe	−54.0	−58.8	**−61.0**	−54.1	−54.7	−58.5	−63.5[b]
Zn	−46.9	−51.5	**−53.7**	−47.0	−47.8	−51.0	−56.2[b]
Ar^{8+}	**−41.0**	−46.1	−48.5	−41.4	−42.1	−44.9	−39.9[a]
Ar^{6+}	−38.3	−43.2	−45.6	−38.7	−39.6	**−42.2**	−41.3[a]
C^{2+}	−24.0	−27.7	**−29.6**	−24.5	−25.7	−24.9	−35.1[a]
N^{3+}	−24.7	−28.6	**−30.5**	−25.2	−26.4	−25.8	−35.1[a]
O^{4+}	−25.3	−29.2	**−31.2**	−25.7	−26.9	−26.4	−38.5[a]
MAE	5.3	**4.2**	4.4	5.2	4.8	**4.2**	
MARE	0.13	0.12	0.14	0.13	0.12	**0.11**	
			Spin–polarized atoms and ions				
H	−6.0	−7.2	−7.9	**0.0**	**0.0**	**0.0**	0.0
Ne^{7+}	−19.4	−23.2	−25.2	−18.8	−19.5	**−18.5**	−17.0[a]
Be^{+}	−18.0	−21.3	−23.0	−17.4	−18.3	**−16.9**	−15.8[a]
Li	−17.2	−20.2	−21.7	−16.5	−17.5	**−16.0**	−15.1[a]
Ar^{15+}	−19.6	−23.7	−25.8	−19.0	−19.7	**−18.8**	−17.4[a]
C^{3+}	−18.9	−22.5	−24.3	−18.2	−19.1	**−17.8**	−16.5[a]
N^{4+}	−19.0	−22.8	−24.7	−18.4	−19.3	**−18.0**	−16.7[a]
B^{2+}	−18.6	−22.0	−23.8	−17.9	−18.8	**−17.4**	−16.2[a]
O^{+}	−27.1	−30.8	−32.6	**−27.9**	−29.0	−28.6	−27.7[a]
O^{5+}	−19.2	−23.0	−24.9	−18.6	−19.4	**−18.2**	−16.8[a]
N	−25.9	−29.3	−31.0	−26.5	−27.7	**−27.0**	−26.9[a]
MAE[c]	2.0	5.3	7.1	1.4	2.2	**1.1**	
MARE[c]	0.12	0.31	0.41	0.08	0.13	**0.07**	

[a]Reference 61.
[b]Reference 62.
[c]Does not include H atom.

constructing the jellium-surface-meta-GGA. This new JS functional is almost exact for jellium surfaces, accurate for atoms and ions, and performs remarkably well for the Hooke's atom of any frequency, including the tightly bounded and strongly correlated regimes.

The JS meta-GGA correlation hole model can be constructed using the reverse engineering method proposed in Ref. 35 for the TPSS case. Because of its good accuracy, our JS meta-GGA correlation energy (and hole) functional can be employed in further research for developing new hyper-GGAs.

Finally, we note that in this work we presented non-self-consistent results, starting from accurate densities, i.e., LSDA for jellium surfaces, Hartree-Fock for atoms and ions, or exact density for the Hooke's atom. This is common procedure for a first assessment of the correlation functional. In a forthcoming paper we will investigate self-consistency effects as well as an appropriate exchange functional to be used together with JS.

ACKNOWLEDGMENTS

This work was partially funded by the European Research Council (ERC) Starting Grant FP7 Project DEDOM, Grant Agreement No. 207441.

[1]W. Kohn and L. J. Sham, Phys. Rev. **140**, A1133 (1965).
[2]R. M. Dreizler and E. K. U. Gross, *Density Functional Theory* (Springer, New York, 1990).
[3]J. P. Perdew and K. Schmidt, in *Density Functional Theory and Its Application to Materials*, edited by V. E. Van Doren, K. Van Alsenoy, and P. Geerlings (American Institute of Physics, Melville, NY, 2001).

[4]J. P. Perdew and Y. Wang, Phys. Rev. B **46**, 12947 (1992).
[5]J. P. Perdew and Y. Wang, Phys. Rev. B **45**, 13244 (1992).
[6]J. P. Perdew, L. A. Constantin, E. Sagvolden, and K. Burke, Phys. Rev. Lett. **97**, 223002 (2006).
[7]A. D. Becke, Phys. Rev. A **38**, 3098 (1988); C. Lee, W. Yang, and R. G. Parr, Phys. Rev. B **37**, 785 (1988).
[8]Y. Zhang and W. Yang, Phys. Rev. Lett. **80**, 890 (1998).
[9]L. A. Constantin, E. Fabiano, S. Laricchia, and F. Della Sala, Phys. Rev. Lett. **106**, 186406 (2011).
[10]J. P. Perdew, K. Burke, and M. Ernzerhof, Phys. Rev. Lett. **77**, 3865 (1996).
[11]J. P. Perdew, A. Ruzsinszky, G. I. Csonka, O. A. Vydrov, G. E. Scuseria, L. A. Constantin, X. Zhou, and K. Burke, Phys. Rev. Lett. **100**, 136406 (2008); **102**, 039902(E) (2008); **101**, 239702 (2008).
[12]R. Armiento and A. E. Mattsson, Phys. Rev. B **72**, 085108 (2005).
[13]E. Fabiano, L. A. Constantin, and F. Della Sala, Phys. Rev. B **82**, 113104 (2010).
[14]J. Tao, J. P. Perdew, V. N. Staroverov, and G. E. Scuseria, Phys. Rev. Lett. **91**, 146401 (2003).
[15]J. P. Perdew, A. Ruzsinszky, G. I. Csonka, L. A. Constantin, and J. Sun, Phys. Rev. Lett. **103**, 026403 (2009).
[16]J. Sun, M. Marsman, A. Ruzsinszky, G. Kresse, and J. P. Perdew, Phys. Rev. B **83**, 121410 (2011).
[17]S. Kümmel and L. Kronik, Rev. Mod. Phys. **80**, 3 (2008).
[18]F. Della Sala and A. Görling, J. Chem. Phys. **115**, 5718 (2001).
[19]E. Fabiano and F. Della Sala, J. Chem. Phys. **126**, 214102 (2007).
[20]J. P. Perdew, V. N. Staroverov, J. Tao, and G. E. Scuseria, Phys. Rev. A **78**, 052513 (2008).
[21]J. Toulouse, I. C. Gerber, G. Jansen, A. Savin, and J. G. Ángyán, Phys. Rev. Lett. **102**, 096404 (2009).
[22]H. V. Nguyen and G. Galli, J. Chem. Phys. **132**, 044109 (2010).
[23]J. Harl and G. Kresse, Phys. Rev. Lett. **103**, 056401 (2009).
[24]J. F. Dobson, J. Wang, and T. Gould, Phys. Rev. B **66**, 081108 (2002).
[25]L. A. Constantin, J. M. Pitarke, J. F. Dobson, A. García-Lekue, and J. P. Perdew, Phys. Rev. Lett. **100**, 036401 (2008).
[26]N. D. Lang and W. Kohn, Phys. Rev. B **1**, 4555 (1970).
[27]J. M. Pitarke and J. P. Perdew, Phys. Rev. B **67**, 045101 (2003).
[28]E. Krotscheck, W. Kohn, and Guo-Xin Qian, Phys. Rev. B **32**, 5693 (1985).
[29]P. H. Acioli and D. M. Ceperley, Phys. Rev. B **54**, 17199 (1996).
[30]B. Wood, N. D. M. Hine, W. M. C. Foulkes, and P. García-González, Phys. Rev. B **76**, 035403 (2007).
[31]J. M. Pitarke, L. A. Constantin, and J. P. Perdew, Phys. Rev. B **74**, 045121 (2006).
[32]D. C. Langreth and J. P. Perdew, Phys. Rev. B **15**, 2884 (1977); **21**, 5469 (1980); **26**, 2810 (1982).
[33]K. Burke, J. P. Perdew, and D. C. Langreth, Phys. Rev. Lett. **73**, 1283 (1994).
[34]Z. Yan, J. P. Perdew, S. Kurth, C. Fiolhais, and L. Almeida, Phys. Rev. B **61**, 2595 (2000).
[35]L. A. Constantin, J. P. Perdew, and J. Tao, Phys. Rev. B **73**, 205104 (2006).
[36]J. M. Pitarke and A. G. Eguiluz, Phys. Rev. B **57**, 6329 (1998); **63**, 045116 (2001).
[37]L. A. Constantin, J. P. Perdew, and J. M. Pitarke, Phys. Rev. B **79**, 075126 (2009).
[38]A. Ruzsinszky, G. I. Csonka, and G. E. Scuseria, J. Chem. Theor. Comput. **5**, 763 (2009).
[39]E. Fabiano, L. A. Constantin, and F. Della Sala, J. Chem. Phys. **134**, 194112 (2011).
[40]J. P. Perdew, J. A. Chevary, S. H. Vosko, K. A. Jackson, M. R. Pederson, D. J. Singh, and C. Fiolhais, Phys. Rev. B **46**, 6671 (1992).
[41]L. M. Almeida, J. P. Perdew, and C. Fiolhais, Phys. Rev. B **66**, 075115 (2002).
[42]I. Sarria, C. Henriques, C. Fiolhais, and J. M. Pitarke, Phys. Rev. B **62**, 1699 (2000).
[43]M. Ernzerhof and J. P. Perdew, J. Chem. Phys. **109**, 3313 (1998).
[44]P. Gori-Giorgi and J. P. Perdew, Phys. Rev. B **66**, 165118 (2002).
[45]J. P. Perdew, K. Burke, and Y. Wang, Phys. Rev. B **54**, 16533 (1996).
[46]J. P. Perdew, H. Q. Tran, and E. D. Smith, Phys. Rev. B **42**, 11627 (1990).
[47]J. P. Perdew, Y. Wang, and E. Engel, Phys. Rev. Lett. **66**, 508 (1991).
[48]P. Giannozzi *et al.*, J. Phys.: Condens. Matter **21**, 395502 (2009).
[49]N. E. Singh-Miller and N. Marzari, Phys. Rev. B **80**, 235407 (2009).
[50]R. Gaudoin, W. M. C. Foulkes, and G. Rajagopal, J. Phys.: Condens. Matter **14**, 8787 (2002).
[51]R. Gaudoin and W. M. C. Foulkes, Phys. Rev. B **66**, 052104 (2002).
[52]G. I. Csonka, J. P. Perdew, A. Ruzsinszky, P. H. T. Philipsen, S. Lebègue, J. Paier, O. A. Vydrov, and J. G. Ángyán, Phys. Rev. B **79**, 155107 (2009).
[53]J. P. Perdew, J. Tao, V. N. Staroverov, and G. E. Scuseria, J. Chem. Phys. **120**, 6898 (2004).
[54]J. P. Perdew, S. Kurth, A. Zupan, and P. Blaha, Phys. Rev. Lett. **82**, 2544 (1999).
[55]C. D. Hu and D. C. Langreth, Phys. Rev. B **33**, 943 (1986).
[56]Y. Wang and J. P. Perdew, Phys. Rev. B **43**, 8911 (1991).
[57]M. Taut, Phys. Rev. A **48**, 3561 (1993).
[58]C. Filippi, C. J. Umrigar, and M. Taut, J. Chem. Phys. **100**, 1290 (1994).
[59]C. Filippi, X. Gonze, and C. J. Umrigar, in *Recent Developments and Applications of Modern Density Functional Theory*, Theoretical and Computational Chemistry Vol. 4, edited by J. M. Seminario (Elsevier, Amsterdam, 1996).
[60]E. Clementi and C. Roetti, At. Data Nucl. Data Tables **14**, 177 (1974).
[61]E. R. Davidson, S. A. Hagstrom, S. J. Chakravorty, V. M. Umar, and C. F. Fischer, Phys. Rev. A **44**, 7071 (1991); S. J. Chakravorty, S. R. Gwaltney, E. R. Davidson, F. A. Parpia, and C. F. Fischer, *ibid.* **47**, 3649 (1993).
[62]E. Clementi and G. Corongiu, Int. J. Quantum Chem. **62**, 571 (1997).
[63]L. A. Constantin and J. M. Pitarke, Phys. Rev. B **83**, 075116 (2011).
[64]C. M. Horowitz, C. R. Proetto, and J. M. Pitarke, Phys. Rev. B **81**, 121106 (2010).